Brownian Asymmetric Simple Exclusion Process

Dominik Lips,[1,*] Artem Ryabov,[2,†] and Philipp Maass[1,‡]
[1]Universität Osnabrück, Fachbereich Physik, Barbarastraße 7, D-49076 Osnabrück, Germany
[2]Charles University, Faculty of Mathematics and Physics, Department of Macromolecular Physics, V Holešovičkách 2, CZ-18000 Praha 8, Czech Republic

(Received 29 June 2018; published 16 October 2018)

We study the driven Brownian motion of hard rods in a one-dimensional cosine potential with a large amplitude compared to the thermal energy. In a closed system, we find surprising features of the steady-state current in dependence of the particle density. The form of the current-density relation changes greatly with the particle size and can exhibit both a local maximum and minimum. The changes are caused by an interplay of a barrier reduction, blocking, and exchange symmetry effect. The latter leads to a current equal to that of noninteracting particles for a particle size commensurate with the period length of the cosine potential. For an open system coupled to particle reservoirs, we predict five different phases of nonequilibrium steady states to occur. Our results show that the particle size can be of crucial importance for nonequilibrium phase transitions in driven systems. Possible experiments for demonstrating our findings are pointed out.

DOI: 10.1103/PhysRevLett.121.160601

A minimal model for studying fundamental questions of nonequilibrium physics is the asymmetric simple exclusion process (ASEP) [1,2], which is sometimes referred to as the "Ising model of nonequilibrium statistical mechanics" [3]. In this model, particles with exclusion interaction hop between neighboring sites of a one-dimensional lattice with a bias in one direction. Many intriguing findings were reported for this ASEP, as exact results for microstate distributions in nonequilibrium steady states (NESSs) [4], phase transitions of NESSs [5–7], condensation transitions in systems with random [8] and non-Poissonian hopping rates [9], and singular points in rate functions characterizing large deviations of fluctuations in time-averaged currents [10–12].

Most applications of the ASEP are found in the modeling of biological traffic [13,14], where the model was first introduced to describe protein synthesis by ribosomes [15] and where it is frequently used now in studies of molecular motor motion [16,17]. Clearly, refinements of the core model are needed for corresponding applications, such as inhomogeneous hopping rates, particles occupying several sites, internal states of particles, and multilane variants [13,14,16,17]. A direct comparison of models and experiments in this area, however, is difficult to realize and hampered by the complexity of biological transport phenomena.

Here, we consider a Brownian motion of particles with the following ingredients resembling features of the ASEP: (i) an exclusion interaction between particles over a range σ, (ii) a periodic potential $U(x)$ with period length λ, giving rise to an effective hopping motion of the particles between the potential wells, and (iii) a constant drag force f acting on the particles. This Brownian ASEP (BASEP) is a broadly applicable model for one-dimensional transport processes [18] with their ubiquitous occurrence in, e.g., zeolites [19], nanotubes [20,21], and membrane channels and pores [22–24]. It can be realized in laboratory study using recently proposed combinations of microfluidics and optical micromanipulation techniques [25–27]. Such experiments have a potential to probe and verify fundamental theoretical predictions for nonequilibrium collective phenomena. The lattice ASEP may, due to its discreteness, not be a correct model for such continuous-space dynamics.

Indeed, we show in this Letter that the BASEP exhibits surprising features that have no counterpart in the ASEP. These features are a consequence of the length scale σ, which enters the problem as a parameter in addition to the particle density ρ. The site blocking effect associated with the exclusion interaction dominates the steady-state particle current $j(\rho,\sigma)$ in a limited σ range only. Because of a barrier reduction effect, $j(\rho,\sigma)$ can be larger than the current $j_0(\rho)$ of noninteracting particles. An exchange symmetry effect emerges when σ becomes commensurate with the period length λ. In this case $j(\rho,\sigma=\lambda)=j_0(\rho)$, as if there were no interactions. The interplay of the barrier reduction, blocking, and exchange symmetry effects leads to changes of the form of the current-density relation with the particle size. This in turn leads to the appearance of five different nonequilibrium phases in open BASEPs coupled to particle reservoirs.

Figure 1 illustrates interacting particles of size σ that are driven by a drag force f through a cosine potential $U(x)=(U_0/2)\cos(2\pi x/\lambda)$ with barrier height U_0. Their center of mass positions x_i, $i=1,\ldots,N$, are considered to perform

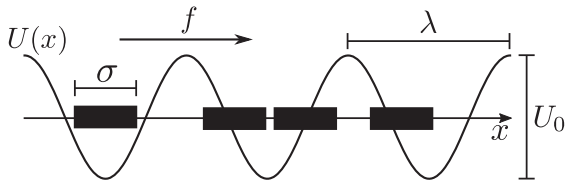

FIG. 1. Driven Brownian motion of interacting particles of size σ in a cosine potential with barrier height U_0 and period length λ under drag force f.

an overdamped Brownian motion according to the coupled Langevin equations

$$\frac{dx_i}{dt} = \mu[f^{\text{ext}}(x_i) + f_i^{\text{int}}] + \sqrt{2D}\eta_i(t), \tag{1}$$

where $f^{\text{ext}}(x) = f - dU(x)/dx$ is the external force, $f_i^{\text{int}} = f_i^{\text{int}}(x_1, \ldots, x_N)$ is the interaction force on the ith particle, and $\eta_i(t)$ are independent Gaussian white noise processes with zero mean and $\langle \eta_i(t)\eta_j(t')\rangle = \delta_{ij}\delta(t-t')$; μ and $D = k_BT\mu$ are the bare mobility and diffusion coefficient, respectively, and k_BT is the thermal energy. In the BASEP, f_i^{int} is solely determined by the hard-core exclusion between neighboring particles, i.e., a contribution upon particle contact. The system size L is taken to be an integer multiple of λ and periodic boundary conditions are imposed. As units for length, time, and energy, we choose λ, λ^2/D, and k_BT, respectively. The density, or filling factor, is $\rho = N/L$. We set $U_0 \gg k_BT$ to generate an effective hopping motion of the particles and focus first on the case where both ρ and σ lie in the range [0, 1].

To determine $j(\rho,\sigma)$ in the nonequilibrium steady state (NESS), we have carried out Brownian dynamics simulations, which we corroborate by analytical considerations. The barrier height and the drag force are fixed by setting $U_0 = U_0/(k_BT) = 6$ and $f = f\lambda/(k_BT) = 1$. In most of the simulations, we have chosen $L = 100$. For ρ and σ close to one, simulations were performed also for larger L to check that our results are not affected by the finite system size. The hard-core interaction force between neighboring particles was simulated according to the algorithm developed in [28]. For σ close to one, we also used the method proposed in [29].

For noninteracting particles, the current increases linearly with ρ, $j_0 = v_0\rho$, where v_0 is the mean velocity of a single particle and can be calculated analytically [30]; for our parameters, $v_0 \cong 0.043$. By the hard-core interaction, this linear current-density relation is modified in quite different ways for different particle sizes σ, as can be seen from Fig. 2(a). As reference curves, we included the line $j_0 = v_0\rho$ for noninteracting particles (solid black line) and the corresponding one for the ASEP [1,2], $j_{\text{ASEP}}(\rho) = j_0(\rho)(1-\rho) = v_0\rho(1-\rho)$ (dashed line). Remarkably, the parabolic curve of the ASEP is resembled in a quite limited σ range only.

To understand the nonlinear current-density relation for different particle sizes, it is helpful to first consider the relative current change $\Delta j(\rho,\sigma) = [j(\rho,\sigma) - j_0(\rho)]/j_0(\rho)$ due to the interactions as a function of σ for several fixed ρ. Corresponding curves plotted in Fig. 2(b) show a similar behavior for all ρ. For small σ, Δj increases with σ up to a maximum and then it decreases until crossing the zero line at a value $\sigma_\times(\rho)$. Hence, for $0 < \sigma < \sigma_\times(\rho)$, $j(\rho,\sigma)$ becomes enhanced compared to $j_0(\rho)$. When increasing σ beyond $\sigma_\times(\rho)$, Δj first decreases, then remains approximately constant in a plateaulike regime, and eventually increases again, where $\Delta j = 0$ for $\sigma = 1$ and all ρ. Hence,

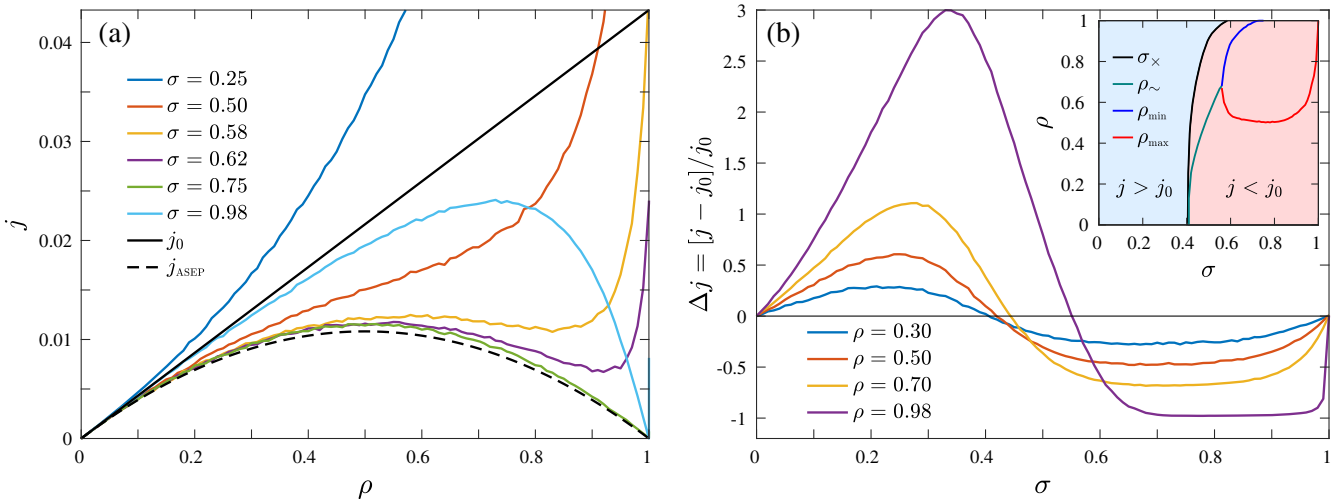

FIG. 2. (a) Current-density relations for various fixed particle sizes σ. The solid and dashed black lines mark the currents $j_0(\rho)$ and $j_{\text{ASEP}}(\rho)$ for noninteracting particles and the corresponding ASEP, respectively. (b) Particle size dependence of the current change $\Delta j(\rho,\sigma) = [j(\rho,\sigma) - j_0(\rho)]/j_0(\rho)$ due to hard-core interactions for different fixed densities ρ. (Inset) The curve $\sigma_\times(\rho)$, which separates the region of current enhancement (blue area) and reduction (red area) and the dependence of $\rho_\sim$, $\rho_{\max}$, and $\rho_{\min}$ on σ.

$j(\rho,\sigma)$ becomes reduced compared to $j_0(\rho)$ for $\sigma_\times(\rho) < \sigma < 1$, and it becomes equal to j_0 for $\sigma = 1$. The crossover value $\sigma_\times(\rho)$ increases with ρ and the full curve shown in the inset of Fig. 2(b) divides the $\sigma - \rho$ plane in two regions of current enhancement and reduction.

The enhancement of the current is caused by a barrier reduction effect, which occurs if a potential well is occupied by more than one particle [31]. Inside a multioccupied well, the mutually excluding particles exhibit, on average, higher potential energies than a particle in a single-occupied well. They need to surmount a lower barrier for escaping the well, which causes the current enhancement. This enhancement is stronger with larger ρ [see Fig. 2(b)], because the probability of multioccupancies rises with increasing ρ. Also, clusters of neighboring occupied wells become larger on average. This facilitates a cascade-like propagation of multioccupations, as demonstrated in Fig. 3(a).

With increasing σ, the formation of multiple occupancies requires higher energies and becomes less likely. For $\sigma > \sigma_\times(\rho)$, the blocking effect, known from the ASEP, prevails. It means that an effective particle hopping to a neighboring well is suppressed if the target well is occupied. Typical particle trajectories in this regime, displayed in Fig. 3(b), show that clusters of neighboring particles frequently move in a manner where wells are sequentially vacated and filled. Hence, the particle motion becomes similar to a hopping on a lattice with forbidden multioccupation of sites. The current then is nearly independent of σ, as reflected in the plateaulike σ intervals in Fig. 2(b).

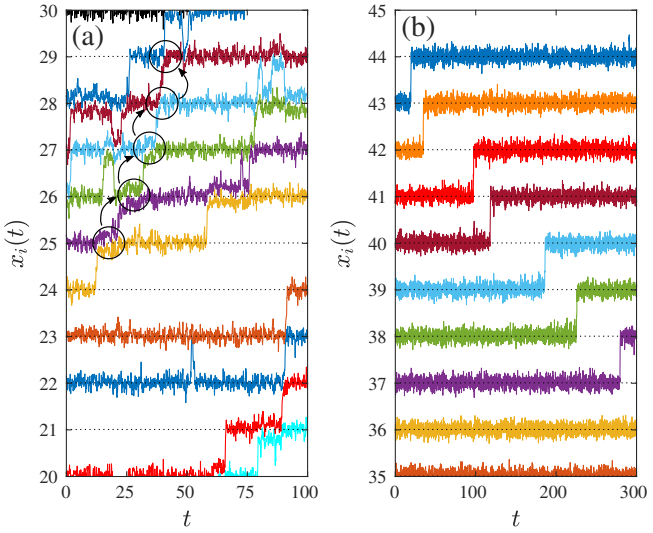

FIG. 3. Particle trajectories in the BASEP for $\rho = 0.75$, and (a) $\sigma = 0.25$ and (b) $\sigma = 0.75$. The horizontal dotted lines indicate the positions of the potential minima. (a) A cascadelike propagation of double occupancies marked by the circles is demonstrated by the arrows. (b) Potential wells are vacated and filled in a sequential process.

To understand why the current increases again for σ approaching one, let us consider a coordinate transformation $x_i \to x_i' = x_i - i\sigma$ in the Langevin equations (1), which for $\sigma = \lambda = 1$ leaves them invariant because of the λ periodicity of $f^{\mathrm{ext}}(x)$. After this transformation, the dynamics of the x_i' correspond to that of point particles. However, for point particles with hard-core interaction, collective properties, like the current, become invariant under particle exchange [32] and, accordingly, $j(\rho,1) = j_0(\rho)$ for all ρ. Refining this line of reasoning, we show in the Supplemental Material [33] that the current for general $\sigma \geq \lambda$ can be inferred from that for $\sigma < \lambda$.

All results are further supported by analytical calculations when starting from the Smoluchowski equation for the joint probability density $p_N(x_1,\ldots,x_N,t)$ of finding the particles at positions $x_1,\ldots,x_N$ at time t [33]. In the NESS, we obtain

$$j(\rho,\sigma) = \left(\mu(f^{\mathrm{ext}}(x) + \langle f^{\mathrm{int}}(x)\rangle) - D\frac{d}{dx}\right)\rho_{\mathrm{loc}}(x), \quad (2)$$

where $\rho_{\mathrm{loc}}(x)$ is the local density and

$$\langle f^{\mathrm{int}}(x)\rangle = k_B T[\psi_-(x) - \psi_+(x)] \quad (3)$$

is the mean interaction force on a particle at position x. Here, $\psi_-(x) = \Psi_-(x)/\rho_{\mathrm{loc}}(x)$ and $\psi_+(x) = \Psi_+(x)/\rho_{\mathrm{loc}}(x)$ are the conditional probability densities that, given a particle at position x, a neighboring particle is in contact (at distance σ) with it in counterclockwise and clockwise directions, respectively; $\Psi_\pm(x)$ are the respective joint probability densities. Because $\Psi_-(x) = \Psi_+(x)$ for $\sigma = \lambda$, it holds that $\langle f^{\mathrm{int}}(x)\rangle = 0$ for $\sigma = \lambda = 1$ from Eq. (3), and it follows that $j(\rho,1) = j_0(\rho)$ from Eq. (2).

Moreover, multiplying Eq. (2) with $1/\rho_{\mathrm{loc}}(x)$ and integrating over one period λ, we obtain, when utilizing the λ periodicity of $\rho_{\mathrm{loc}}(x)$ in the NESS and of $U(x)$ in $f^{\mathrm{ext}}(x) = f - dU(x)/dx$,

$$j(\rho,\sigma) = \frac{\mu(f + \bar{f}^{\mathrm{int}})\lambda}{\int_0^\lambda \frac{dx}{\rho_{\mathrm{loc}}(x)}}, \quad (4)$$

where $\bar{f}^{\mathrm{int}} = \lambda^{-1}\int_0^\lambda dx\langle f^{\mathrm{int}}(x)\rangle$ is the period-averaged mean interaction force. This exact expression for the current is analogous to the corresponding one for a single particle [30], but here it refers to a many-body system with hard-core interactions, where $\bar{f}^{\mathrm{int}}$ gives an additional contribution to the driving force. In fact, Eq. (4) is valid also for other interaction forces if the corresponding mean interaction force is used. We further give in the Supplemental Material [33] an approximate treatment of Eq. (4) for weak bias, which reproduces qualitatively the behavior shown in Figs. 2(a) and 2(b).

Let us now discuss the curves in Fig. 2(a) with increasing σ. For small $\sigma = 0.25$, $j(\rho,\sigma)$ is larger than $j_0(\rho)$ and

increases monotonically due to the barrier reduction effect. Enlarging σ, the blocking effect becomes more relevant, which causes the curves to approach more and more $j_{\mathrm{ASEP}}(\rho)$. First, this leads to a change of curvature of $j(\rho,\sigma)$ from concave to convex at a density $\rho=\rho_{\sim}$ (see the curve for $\sigma=0.5$). Then, when σ exceeds a critical value $\sigma_c\cong 0.55$, a local maximum at $\rho=\rho_{\max}$ and a local minimum at $\rho=\rho_{\min}$ occurs (see the curves for $\sigma=0.58$ and $\sigma=0.62$). Upon further increasing σ, a range of particle sizes appears, where $j(\rho,\sigma)\simeq j_{\mathrm{ASEP}}(\rho)$. Eventually, the exchange symmetry effect becomes noticeable, which causes $j(\rho,\sigma)$ to approach $j_0(\rho)$. Going along with this is a shift of the local maximum $\rho_{\max}$ and of $j(\rho_{\max},\sigma)$ towards larger values (see the curve for $\sigma=0.98$). The dependence of $\rho_{\sim}$, $\rho_{\max}$, and $\rho_{\min}$ on σ is shown in the inset of Fig. 2(b).

The different forms of the current-density relation lead to a versatile emergence of NESS phases in an open BASEP in contact with two particle reservoirs at its left and right end. In this open BASEP, the period-averaged densities $\bar{\rho}_i=\lambda^{-1}\int_{(i-1)\lambda}^{i\lambda}dx\rho_{\mathrm{loc}}(x)$ in each well $i=1,\ldots,L/\lambda$ are no longer equal, but approach a constant "bulk value" ρ_b in the system's interior, far from the boundaries. This bulk density ρ_b or its derivative can change abruptly upon variation of the system-reservoir couplings, i.e., the parameters controlling the particle exchange with the reservoirs. The corresponding sets of phase transition points separate NESS phases, in which the order parameter ρ_b varies smoothly with the system-reservoir couplings.

Independent of the details of the couplings, all possible NESS phases can be uncovered from $j(\rho,\sigma)$ by considering just two control parameters $\rho_L,\rho_R\in[0,1]$, which for *bulk-adapted* couplings represent the particle densities in the left and right reservoir, respectively [41–43]. The different phases are obtained by applying the extremal current principles [5,44], which state that ρ_b assumes the value at which $j(\rho,\sigma)$ becomes minimal (for $\rho_L<\rho_R$) or maximal (for $\rho_R<\rho_L$) in the ρ intervals enclosed by ρ_L and ρ_R,

$$\rho_b=\begin{cases}\mathrm{argmin}_{\rho_L\le\rho\le\rho_R}\{j(\rho,\sigma)\}, & \rho_L\le\rho_R,\\ \mathrm{argmax}_{\rho_R\le\rho\le\rho_L}\{j(\rho,\sigma)\}, & \rho_R\le\rho_L.\end{cases}\tag{5}$$

For $\sigma<\sigma_c$, the extremal current principles in Eq. (5) imply that no phase transitions occur in the open BASEP, because $j(\rho,\sigma)$ exhibits no local minima or maxima. For $\sigma>\sigma_c$, by contrast, phase transitions occur and we show in Fig. 4 different examples of phase diagrams of NESSs. Dashed and solid lines in these diagrams indicate phase transitions of first and second order, respectively.

In Fig. 4(a), $\sigma=0.58$ is close to σ_c and in total five NESS phases appear. For the left-boundary induced phases I and V, $\rho_b=\rho_L$, and for the right-boundary induced phase III, $\rho_b=\rho_R$; phase II is a maximal current phase with $\rho_b=\rho_{\max}\cong 0.60$ and phase IV is a minimal current phase with $\rho_b=\rho_{\min}\cong 0.83$ [see Fig. 2(a)]. With increasing σ, the phase regions II–IV extend, while the regions I and V shrink [see Fig. 4(b)]. We note that the topology of the phase diagrams in Figs. 4(a) and 4(b) resembles features seen in corresponding phase diagrams of driven lattice gases with repulsive nearest-neighbor interactions [41,43,44]. For the phase diagram in Fig. 4(b), we demonstrate the occurrence of different NESS phases in simulations of an open BASEP in the Supplemental Material [33].

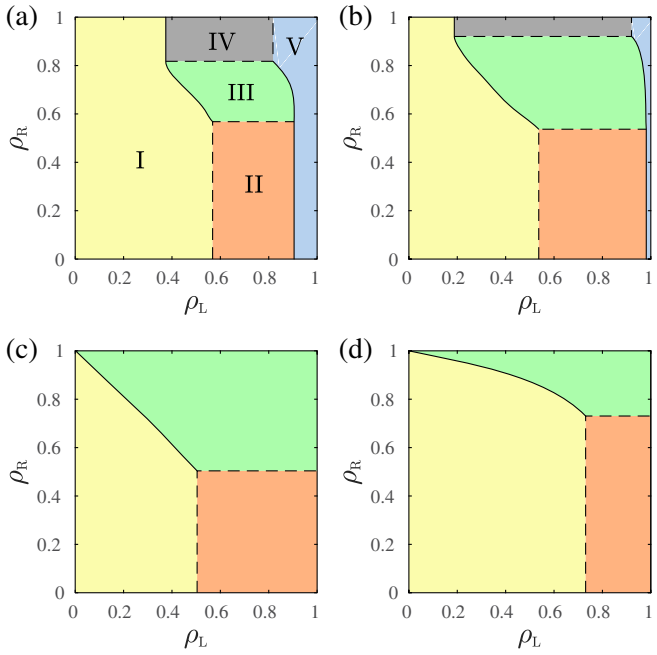

FIG. 4. Phase diagrams of the open BASEP for particle sizes (a) $\sigma=0.58$, (b) $\sigma=0.62$, (c) $\sigma=0.75$, and (d) $\sigma=0.98$. Dashed and solid lines indicate phase transitions of first and second order, respectively. The regions labeled I–V in (a) mark two left-boundary induced phases (I and V), a right-boundary induced phase (III), a maximal current phase (II), and a minimal current phase (IV). These phases are equally colored in all graphs.

When entering the σ regime, where $j(\rho,\sigma)\simeq j_{\mathrm{ASEP}}(\rho)$, the phase diagram resembles that of the ASEP with phases I–III, as shown in Fig. 4(c) [45]. Finally, when the exchange symmetry effect causes $\rho_{\max}$ to approach one, phase regions II and III shrink at the expense of region I [see Fig. 4(d)].

To conclude, the interplay of the barrier reduction, blocking, and exchange symmetry effects gives rise to a surprisingly versatile form of the current-density relation in the BASEP in dependence of the particle size. This leads us to predict the appearance of in total five different phases of NESS states in the open BASEP coupled to particle reservoirs. Only for a quite limited range of particle sizes is the behavior of the BASEP resembled by the ASEP.

Similar nonequilibrium phase transitions as in the BASEP are expected to occur for particles with soft repulsive interactions of short range. Indeed, we could identify these in simulations with a Yukawa interaction. For

a power-law soft core, just an ASEP-like behavior was reported earlier [46].

Besides its relevance in biology, where confined transport processes through channels with binding sites [22–24] are mediated by driven Brownian motion, we believe that the BASEP is an ideal *in situ* tunable model system for an experimental exploration of nonequilibrium phase transitions. Current experimental micromanipulation techniques allow precise engineering and fine tuning of relevant aspects of the model: the external tilted periodic potential and the confinement. The precise control of the potential may be achieved with high precision using holographic optical tweezers as it was done in a related experimental work [25]. The confinement can be realized within microfluidic chips. Combining microfluidics with optical tweezers already proved to be a realizable method to probe fundamentals of facilitated diffusion in confined spaces [47,48] and of escape times in single-file transport [49]. Another intriguing recent option is to consider a nanofluidic ratchet [26,27], where the periodic potential landscape is shaped by the geometry of a nanofluidic slit and an additional electrostatic interaction between particles and walls.

This work has been funded by the Deutsche Forschungsgemeinschaft (MA 1636/10-1), the Czech Science Foundation (Project No. 17-06716S), the DAAD (57336032), and the MŠMT (7AMB17DE014). We sincerely thank W. Dieterich and the members of the DFG Research Unit FOR 2692 for fruitful discussions.

*dlips@uos.de
†rjabov.a@gmail.com
‡maass@uos.de

[1] B. Derrida, Phys. Rep. **301**, 65 (1998).
[2] G. M. Schütz, in *Phase Transitions and Critical Phenomena*, edited by C. Domb and J. Lebowitz (Academic Press, London, 2001), Vol. 19, p. 1.
[3] B. Schmittmann and R. K. P. Zia, in *Phase Transitions and Critical Phenomena*, edited by C. Domb and J. Lebowitz (Academic Press, London, 1995), Vol. 17.
[4] R. A. Blythe and M. R. Evans, J. Phys. A **40**, R333 (2007).
[5] J. Krug, Phys. Rev. Lett. **67**, 1882 (1991).
[6] A. Parmeggiani, T. Franosch, and E. Frey, Phys. Rev. Lett. **90**, 086601 (2003).
[7] A. B. Kolomeisky, J. Phys. A **31**, 1153 (1998).
[8] M. R. Evans, Europhys. Lett. **36**, 13 (1996).
[9] R. J. Concannon and R. A. Blythe, Phys. Rev. Lett. **112**, 050603 (2014).
[10] L. Bertini, A. De Sole, D. Gabrielli, G. Jona-Lasinio, and C. Landim, Phys. Rev. Lett. **94**, 030601 (2005).
[11] A. Lazarescu, J. Phys. A **48**, 503001 (2015).
[12] Y. Baek, Y. Kafri, and V. Lecomte, Phys. Rev. Lett. **118**, 030604 (2017).
[13] A. Schadschneider, D. Chowdhury, and K. Nishinari, *Stochastic Transport in Complex Systems: From Molecules to Vehicles*, 3rd ed. (Elsevier Science, Amsterdam, 2010).
[14] T. Chou, K. Mallick, and R. K. P. Zia, Rep. Prog. Phys. **74**, 116601 (2011).
[15] C. T. MacDonald, J. H. Gibbs, and A. C. Pipkin, Biopolymers **6**, 1 (1968).
[16] A. B. Kolomeisky, J. Phys. Condens. Matter **25**, 463101 (2013).
[17] C. Appert-Rolland, M. Ebbinghaus, and L. Santen, Phys. Rep. **593**, 1 (2015).
[18] A. Taloni, O. Flomenbom, R. Castañeda-Priego, and F. Marchesoni, Soft Matter **13**, 1096 (2017).
[19] K. Hahn, J. Kärger, and V. Kukla, Phys. Rev. Lett. **76**, 2762 (1996).
[20] C.-Y. Cheng and C. R. Bowers, ChemPhysChem **8**, 2077 (2007).
[21] M. Dvoyashkin, H. Bhase, N. Mirnazari, S. Vasenkov, and C. R. Bowers, Anal. Chem. **86**, 2200 (2014).
[22] W. R. Bauer and W. Nadler, Proc. Natl. Acad. Sci. U.S.A. **103**, 11446 (2006).
[23] M. Kahms, P. Lehrich, J. Hüve, N. Sanetra, and R. Peters, Traffic **10**, 1228 (2009).
[24] P. C. Bressloff and J. M. Newby, Rev. Mod. Phys. **85**, 135 (2013).
[25] A. V. Arzola, M. Villasante-Barahona, K. Volke-Sepúlveda, P. Jákl, and P. Zemánek, Phys. Rev. Lett. **118**, 138002 (2017).
[26] M. J. Skaug, C. Schwemmer, S. Fringes, C. D. Rawlings, and A. W. Knoll, Science **359**, 1505 (2018).
[27] C. Schwemmer, S. Fringes, U. Duerig, Y. K. R. Cho, and A. W. Knoll, Phys. Rev. Lett. **121**, 104102 (2018).
[28] H. Behringer and R. Eichhorn, J. Chem. Phys. **137**, 164108 (2012).
[29] A. Scala, T. Voigtmann, and C. De Michele, J. Chem. Phys. **126**, 134109 (2007).
[30] V. Ambegaokar and B. I. Halperin, Phys. Rev. Lett. **22**, 1364 (1969).
[31] A well is n times occupied, if exactly n of the particles' center positions lie in the x interval between the successive potential maxima enclosing the well.
[32] A. Ryabov and P. Chvosta, Phys. Rev. E **83**, 020106 (2011).
[33] See Supplemental Material at http://link.aps.org/supplemental/10.1103/PhysRevLett.121.160601 for details of analytical calculations and comparison with simulation results, which includes Refs. [34–40].
[34] J. K. Percus, J. Stat. Phys. **15**, 505 (1976).
[35] A. R. Bishop, W. Dieterich, and I. Peschel, Z. Phys. B **33**, 187 (1979).
[36] W. Dieterich, P. Fulde, and I. Peschel, Adv. Phys. **29**, 527 (1980).
[37] U. M. B. Marconi and P. Tarazona, J. Chem. Phys. **110**, 8032 (1999).
[38] H. Löwen and M. Heinen, Eur. Phys. J. Spec. Top. **223**, 3113 (2014).
[39] G. Lakatos and T. Chou, J. Phys. A **36**, 2027 (2003).
[40] L. Dagdug and A. M. Berezhkovskii, J. Chem. Phys. **131**, 056101 (2009).
[41] J. S. Hager, J. Krug, V. Popkov, and G. M. Schütz, Phys. Rev. E **63**, 056110 (2001).
[42] M. Dierl, P. Maass, and M. Einax, Phys. Rev. Lett. **108**, 060603 (2012).

[43] M. Dierl, M. Einax, and P. Maass, Phys. Rev. E **87**, 062126 (2013).
[44] V. Popkov and G. M. Schütz, Europhys. Lett. **48**, 257 (1999).
[45] Five NESS phases as in Figs. 4(a) and 4(b) would appear when allowing for filling factors ρ larger than one as a result of an extension of the current-density relation in Fig. 2(a) to the regime $1 < \rho < 1/\sigma$. This regime will be discussed elsewhere.
[46] J. Eduardo de Oliveira Rodrigues and R. Dickman, Phys. Rev. E **81**, 061108 (2010).
[47] S. Pagliara, C. Schwall, and U. F. Keyser, Adv. Mater. **25**, 844 (2013).
[48] S. Pagliara, S. L. Dettmer, and U. F. Keyser, Phys. Rev. Lett. **113**, 048102 (2014).
[49] E. Locatelli, M. Pierno, F. Baldovin, E. Orlandini, Y. Tan, and S. Pagliara, Phys. Rev. Lett. **117**, 038001 (2016).